P2.2 SIMULATION OF SOUND PROPAGATION THROUGH HIGH-RESOLUTION ATMOSPHERIC BOUNDARY LAYER TURBULENCE FIELDS

D. Keith Wilson,*[1] Neill P. Symons,[2] Edward G. Patton,[3]
Peter P. Sullivan,[3] David H. Marlin,[4] David F. Aldridge,[2] Vladimir E. Ostashev,[5,6]
Stephen A. Ketcham,[1] Edgar L Andreas,[1] Sandra L. Collier[7]

[1]U.S. Army Cold Regions Research and Engineering Laboratory, Hanover, New Hampshire
[2]Sandia National Laboratories, Albuquerque, New Mexico
[3]National Center for Atmospheric Research, Boulder, Colorado
[4]U.S. Army Research Laboratory, White Sands Missile Range, New Mexico
[5]NOAA Environmental Technology Laboratory, Boulder, Colorado
[6]New Mexico State University, Las Cruces, New Mexico
[7]U.S. Army Research Laboratory, Adelphi, Maryland

1. INTRODUCTION

Most current numerical methods for predicting sound propagation outdoors, such as the fast field program (FFP) and parabolic equation (PE), are based on approximations to the full wave equation that hinder, or even do not allow, simulating complex propagaton phenomena such as dynamic scattering by atmospheric fields, moving source distributions, and reflections from trees and buildings. [The reader may refer to Attenborough et al. (1995) and Salomons (2001) for detailed discussions of the FFP and PE methods.] In contrast, these propagation phenomena can all be readily handled with finite-difference, time-domain (FDTD) techniques. Recent papers by Blumrich and Heimann (2002) and Salomons et al. (2002) present 2D FDTD calculations for the atmosphere that include sound-blocking barriers in combination with wind and turbulence. Liu and Moran (2002) demonstrated 3D FDTD simulations of propagation in a nonmoving atmosphere with a barrier and dense stand of trees. The main drawback with FDTD, which has so far prevented more widespread use in outdoor sound propagation calculations, is that it is very computationally intensive. As computational capabilities continue to rapidly increase, though, it seems inevitable that FDTD will assume a prominent role in simulating outdoor sound propagation. Full utilization of FDTD will require realistic, high-resolution atmospheric wind and temperature fields as input to capture the dynamic atmospheric structure and random scattering processes that drive acoustic signal variability and coherence.

Atmospheric acoustic FDTD simulations have many practical modeling applications, including noise control in the vicinity of highway barriers and urban structures, atmospheric and terrain effects on outdoor acoustic surveillance sensors, propagation of explosions and sonic booms through the troposphere and stratosphere, and remote sensing systems such as sodar that are based on scattering of sound.

In this paper, we discuss FDTD simulations of sound propagation in the atmosphere and idealized turbulent media. Section 2 describes the time-domain equations that are used to propagate the sound fields and overviews some of the numerical issues involved in their implementation. In Section 3, FDTD is performed with input fields generated by a large-eddy simulation (LES). Section 4 describes FDTD calculations of propagation through turbulence produced by a kinematic method, which is shown to be particularly useful for testing theories of wave scattering by turbulence.

2. ACOUSTIC FDTD IN A MOVING MEDIUM

2.1 *Coupled Equation Set*

Most currently used techniques for calculating sound propagation in the atmosphere (such as the FFP and PE, mentioned in the Introduction) are based on solving the full wave equation or its parabolic approximation. The wave equation is a second-order partial differential equation in both time and space. FDTD techniques, however, are most readily applied to first-order partial differential equations. Furthermore, most solutions of the wave equation have been based on one-way approximations, in which the energy is propagated in only one direction, and on "effective sound-speed" approximations, in which the sound speed is taken to be the actual sound speed plus the component of the wind velocity in the direction of propagation. The wave equation in a moving medium is considerably more complicated than in a stationary medium (Ostashev, 1997). The switch to first-order equations facilitates correct handling of the wind velocity field. The following coupled, first-order equations for the acoustic pressure p and acoustic particle velocity $\mathbf{w}$ involve no one-way or effective sound-speed approximations, and are therefore appropriate starting point for accurate FDTD sound propagation calculations in a moving atmosphere (Ostashev et al., 2004):

$$\frac{\partial p}{\partial t} = -\left(\mathbf{v}\cdot\nabla\right)p - \varrho c^2 \nabla\cdot\mathbf{w} + \varrho c^2 Q, \qquad (1)$$

* *Corresponding author address:* D. Keith Wilson, U.S. Army Cold Regions Research and Engineering Laboratory, 72 Lyme Rd., Hanover, NH 03755-1290; e-mail: D.Keith.Wilson@erdc.usace.army.mil.

$$\frac{\partial \mathbf{w}}{\partial t} = -\left(\mathbf{w}\cdot\nabla\right)\mathbf{v} - \left(\mathbf{v}\cdot\nabla\right)\mathbf{w} - \frac{\nabla p}{\varrho} + \mathbf{F}/\varrho. \quad (2)$$

Here, ρ is medium density, c is the adiabatic speed of sound, and $\mathbf{v}$ is the wind velocity. The quantities $\mathbf{F}$ and Q represent sources: the former is a force acting on the medium, whereas the latter is a mass source. Bold symbols represent vectors. Equations (1) and (2) were derived from the full fluid dynamical equations, subject to the following assumptions: (1) the sound wave is a small perturbation to the background state of the medium, (2) the propagation medium is an incompressible gas (i.e., $\nabla\cdot\mathbf{v} = \mathbf{0}$), (3) the gradient of the background pressure may be neglected, and (4) the Coriolis force may be neglected. These four assumptions are quite typical and reasonable for aeroacoustics. The third may be considered a distinguishing property between sound and gravity waves. An FDTD code based on (1) and (2) would be more general and accurate than most current sound propagation formulations, despite the fairly simple appearance of the differential equations. Numerical issues aside, the density, sound speed, and wind velocity fields specified in (1) and (2) can be arbitrary functions of space and time.

2.2 *Computational Considerations*

Typically, finite-difference solutions for wave propagation in a *nonmoving* medium use a grid that is staggered in space and time (Yee, 1966; Botteldooren, 1994). Each acoustic particle velocity component is explicitly calculated on spatial grid nodes shifted by one-half of the internode spacing, relative to the explicit acoustic pressure nodes, in the direction of the velocity component. The particle velocities and pressures are advanced on alternating time steps. It happens, however, that this "leapfrog" methodology of marching the solution in time cannot be applied directly to Eqs. (1) and (2). Evaluation of the advective terms on the right-hand sides of these equations requires knowledge of the pressure and particle velocity fields at time steps where they are not explicitly available. Therefore, we have developed alternative approaches based on unstaggered temporal grids (Ostashev et al., 2004) and staggered temporal grids spanning multiple time steps (Symons et al., 2003). The latter approach is shown schematically in Figures 1 and 2. The finite-difference stencil shown in these figures involves fully centered finite differences, and is second-order in time and fourth-order in space. As discussed in Wilson and Liu (2004), this approach and several others can yield highly accurate results, although some efficiency in memory usage and/or calculation time is lost in comparison to the customary leapfrog solution for a nonmoving medium.

The size and dimensions of the computational domain in an acoustic FDTD simulation depend on the propagation geometry of interest and the memory available. Artificial sound absorbing layers are placed around the sides and corners of the domain to prevent unwanted numerical reflections. The lower surface is normally taken as a rigid plate, although more sophisticated models with

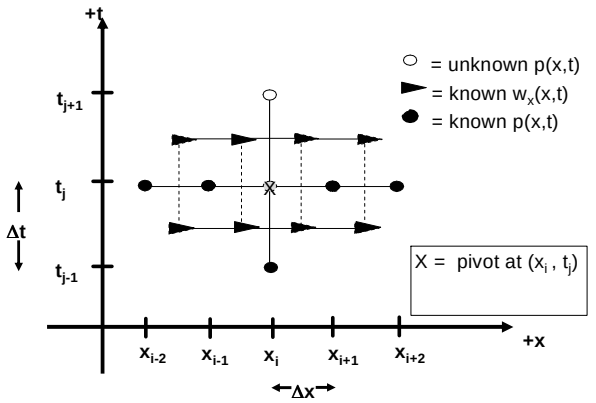

FIG. 1: Staggered finite-diference stencil for updating the acoustic pressure solution in a moving medium. (For simplicity, the stencil is shown with one spatial dimension.)

absorption are under development. The spacing between grid points in acoustic FDTD is driven by the smallest acoustic wavelength of interest. For fourth-order spatial finite-differencing, a typical grid spacing would be 1/8 of the wavelength. As an example of the memory requirements, consider a simulation in which a source emits frequencies at 250 Hz and lower. For a sound speed of 340 m s^{-1}, the minimum wavelength is $340/250 = 1.36$ m, and the grid spacing is therefore 0.17 m. Assuming the dimensions of the computational domain are 500 m in each horizontal direction and 50 m in the vertical, about 2.5×10^9 grid nodes are required. Such intensive computational problems can only be tackled on large, parallel processing computers.

3. ACOUSTIC SIMULATIONS WITH DYNAMIC ATMOSPHERIC MODELS

The time-domain nature of acoustic FDTD makes it a natural approach for coupling with dynamic atmospheric models such as numerical weather predictions (NWP) and atmospheric boundary-layer (ABL) large-eddy simulations (LES). The spatial and temporal resolution of the acoustic FDTD will typically be finer than the LES (since for physical reasons the LES domain normally encompasses the entire ABL, whereas the acoustic FDTD need not) and therefore the LES fields must interpolated in some fashion to the acoustic grid. In this section, we provide examples of FDTD simulations of sound propagating through atmospheric turbulence fields generated by LES.

The LES we use is a parallelized implementation of the physical models and code described in Sullivan et al. (1994) and Sullivan et al. (1996). Two stability cases are considered here. The first is for a neutral ABL (Figure 3) and the second for a buoyantly unstable ABL (Figure 4). Although only the vertical velocity component is shown in these figures, all three velocity components and tempera-

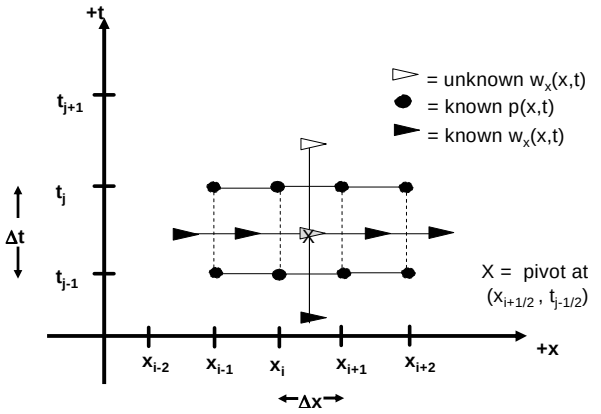

FIG. 2: Staggered finite-diference stencil for updating the acoustic particle velocity solution in a moving medium. (For simplicity, the stencil is shown with one spatial dimension.)

ture were used as input to the acoustic FDTD calculation.

The acoustic calculation was performed with $901 \times 901 \times 603$ grid nodes spaced at 1 m. The time step was 0.25 ms and the solution was advanced over 16001 time steps. Execution required 10 hours on a cluster built from 100 Compaq ES45 processors. The sound source was a 20-Hz, mono-frequency, mass-type source. The middle panels in Figures 3 and 4 show snapshots of the calculated sound fields. Distortions to the propagating wavefronts are not easily discernable in those images. For each case we also propagated sound fields through horizontally averaged LES fields (i.e., the mean vertical profiles only). The difference between the sound fields, with and without the horizontal LES variability, is shown in the lower panels of Figures 3 and 4. The distortions to wavefront shape and amplitude are easily discernable in these difference images. Such distortions impact the ability of acoustical arrays to accurately estimate the bearings of a source and could also potentially be used for atmospheric sensing.

4. ACOUSTIC SIMULATIONS WITH KINEMATIC TURBULENCE

Kinematic turbulence refers here to synthesized random fields that obey a prescribed set of statistics. Usually, the prescribed statistic is a spectrum for the turbulence. Since kinematic turbulence generation does not involve solving the Navier-Stokes equations, it does not realistically capture turbulent dynamics as a simulation such as LES would. However, there are two properties of kinematic turbulence that we regard as particularly useful when it is used in conjunction with the acoustic FDTD. First, because random fields can be synthesized to have a prescribed spectrum, it becomes possible to rigorously test theories for wave propagation through turbulence. Tightly controlled numerical experiments can be conducted that are not contaminated by complicating factors such as refraction, ground reflections, and turbulent anisotropy, which are inevitably present during experiments performed in the atmosphere or a laboratory. The effects of these complicating factors can be explored in controlled combinations, and their relative importance thereby ascertained. Second, it is possible to efficiently parallelize the generation of the kinematic turbulence, thereby allowing turbulence fields to be synthesized quickly and at a much higher resolution than possi-

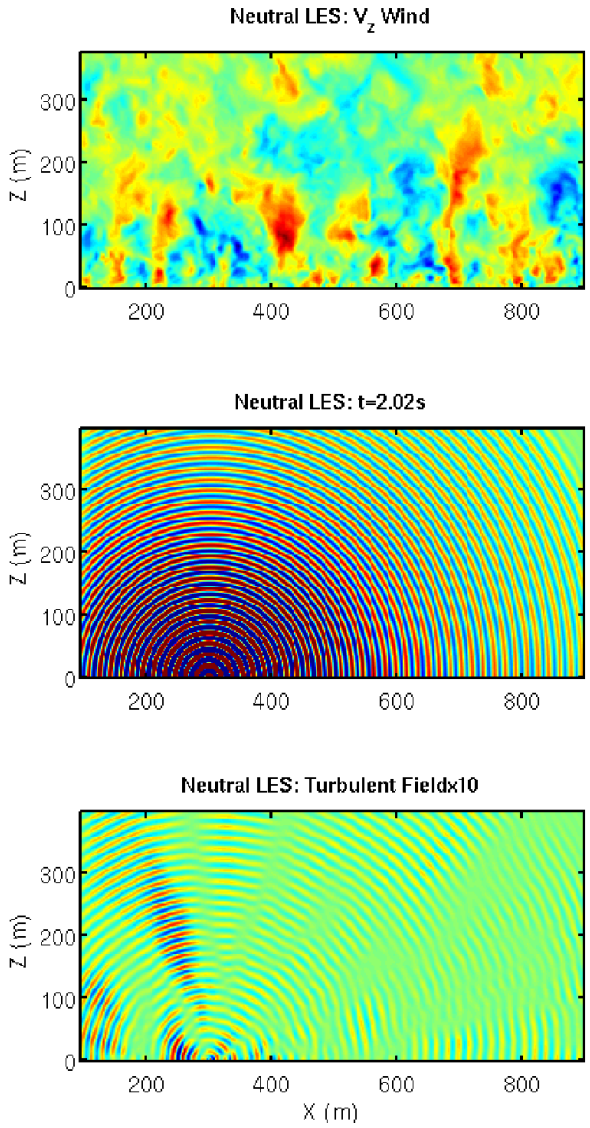

FIG. 3: Top: Vertical wind field from an LES for a neutral ABL ($z_i/L_o = -\infty$). (Only a partial cross section of the LES is shown.) Middle: Acoustic FDTD calculation for an explosive-type source propagating through the neutral LES fields. Bottom: Difference between sound field calculated with turbulence (LES fields) and without turbulence (horizontally averaged LES fields).

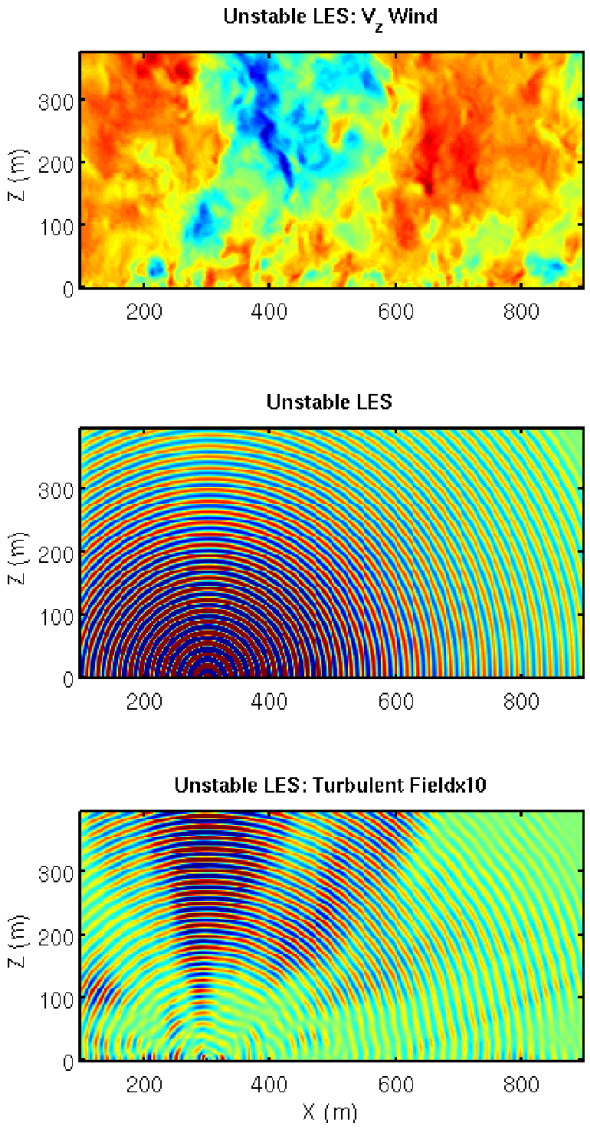

FIG. 4: Same as Figure 3, except for a buoyantly unstable ABL ($z_i/L_o = -6$).

ble with current LES.

Our kinematic turbulence generation method is based on quasi-wavelets (QWs) (Goedecke et al., 2004; Wilson et al., 2004). The QWs are similar to customary wavelets in that they are localized in space and self-similar in scale. However, their positions and orientations are random. The velocity field associated with each QW is given by

$$\mathbf{v}^{\alpha n}(\mathbf{r}) = \mathbf{\Omega}^{\alpha n} \times \left(\mathbf{r} - \mathbf{b}^{\alpha n}\right) \left(-\xi^{-1} \partial f / \partial \xi\right), \qquad (3)$$

where α is an index for the size class, n is a particular QW within that size class, $\mathbf{\Omega}^{\alpha n}$ is the angular velocity, $\mathbf{b}^{\alpha n}$ is the center of the QW, $\mathbf{r}$ is the location in space, $\xi \equiv \left(\mathbf{r} - \mathbf{b}^{\alpha n}\right)/a_\alpha$, and a_α is the size of the QW. The function $f(\xi)$ is the QW parent function, for which in this paper we use a simple Gaussian:

$$f(\xi) = f(0) \exp\left(-\xi^2\right), \qquad (4)$$

The parameters of the QW distribution, including the constant $f(0)$, the number and spacing of the size classes, the angular velocities, and the number density of the QWs, can be chosen in a way that reproduces the Kolmogorov inertial subrange (Goedecke et al., 2004; Wilson et al., 2004). An advantage of using QWs, in comparison to more common Fourier spectral methods, is that the QWs are localized in space. This allows the QW generation to be accomplished with a spatial domain decomposition implemented on a parallel-processing computer. The parallelization is very straight forward and efficient, since each processor needs only to compute the fields associated with the eddies contained within its subdomain. Some QWs, particularly large ones, will span the domains of multiple processors. However, the number of large, processor-spanning QWs is small since the turbulence cascade naturally results in eddies being most numerous at the inner scale of the kinematic turbulence.

Figure 5 shows some example snapshots of kinematic turbulence synthesized by the QW method. The outer scale (a_1) for these kinematic fields is 4 m, and the inner scale (a_N) is 0.5 m. The turbulent kinetic energy dissipation rate was set to ϵ =10 m^{2}s^{-3}. This rather high value was chosen to produce pronounced scattering effects. A total of 4 million QWs were generated. Shown are cross sections through fully 3D kinematic turbulence. These realizations were generated in a cube domain 325 m on a side at a resolution of 0.5, using 216 processors on an IBM SP3 computer. Figure 6 compares the spectra of the synthesized kinematic turbulence to these theoretical forms. The synthesized and theoretical spectra are essentially identical.

Since the synthesized kinematic turbulence fields reproduce turbulence spectra accurately, and the FDTD method propagates wavefields through the turbulence with no approximations beyond the temporal/spatial discretization, these two capabilities when taken together provide an outstanding capability for exploring the validity of theoretical treatments of wave scattering by turbulence. The basic theories in widespread use today were derived, for the most part, in the 1970's. Ishimaru (1978) provides a detailed discussion. More recently, Ostashev (1997) rigorously treated the case of sound-wave propagation through a fluctuating velocity field. As mentioned at the beginning of this section, it is very difficult to ascertain the limits of applicability of these theories because real-world turbulence (in the atmosphere or laboratory) rarely satisfies all of the assumptions made in their derivation.

To address this issue, we performed an acoustic FDTD calculation of propagation through the fields shown in Figure 5. The goal of this particular test was to examine the spatial coherence of the acoustic wavefield. Wavefield coherence is degraded by random perturbations in the propagating wavefronts, which result from

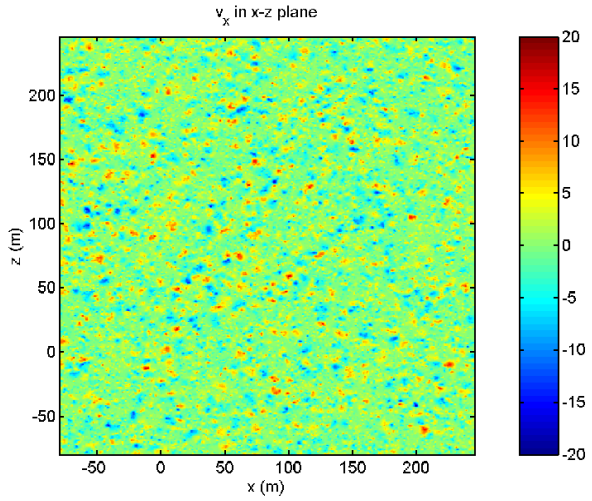

FIG. 5: Kinematic turbulence synthesized by the quasi-wavelet method. Shown is a cross section in the xz-plane through the v_x velocity component. Color scale is in m/s. These fields are used as input for an acoutic FDTD calculation with the source at $(0, 0, 0)$ m.

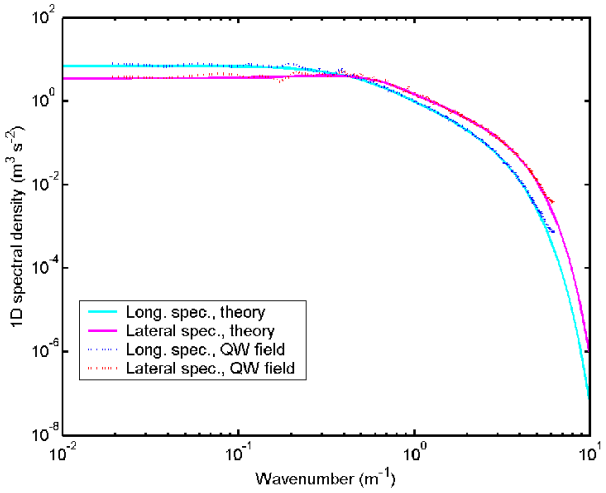

FIG. 6: Comparison of the theoretical 1D longitudinal and lateral spectral densities for the Gaussian QW model with spectra calculated from synthesized turbulence fields such as shown in Figure 5.

spatial variability on the propagation speed and focusing/defocusing by the turbulence. As a result, the signals received by spatially separated sensors (microphones) are imperfectly correlated.

A mono-frequency acoustic source at 100 Hz was used, implying a wavelength of 3.4 m. The duration of the simulation was 2 s and the turbulence was moved as a frozen field at a velocity of 5 m s^{-1}. A total of 500 "virtual microphones" were randomly placed in one spatial quadrant at a distance of 200 m from the source. It would have been impractical to perform an actual experiment with so many microphones. Samples of the complex wavefunction[1] at each sensor are shown in Figure 7. In this representation, variations in signal phase produce sample displacements that are tangent to the unit circle, whereas variations in amplitude produce displacements are perpendicular. Each microphone essentially provides an independent signal sample.

The wavefield coherence $\Gamma(\mathbf{r}) = \langle \psi(\mathbf{r}_0)\, \psi^*(\mathbf{r}_0 + \mathbf{r}) \rangle$ determined from the FDTD results is shown in Figure 8. To make this figure, signals from pairs of virtual microphones with similar spacing were averaged. Also shown on the figure is a theoretical prediction (Ostashev, 1997), based on the parabolic and Markov approximations, for the wavefield coherence during line-of-sight wave propagation. There is a 4% to 6% underprediction of the coherence by the theory. We suspect that the disagreement results from the wavelength being only a little smaller than the outer scale in this case. Stricly speaking, the theory derived in Ostashev (1997) only applies when $a_1 \gg \lambda$. Additional testing of the theory by FDTD simulation, with more frequencies and propagation distances, is planned.

[1] The complex wavefunction is defined as $\psi = \mathbf{p}/\mathbf{p}_0$, where $\mathbf{p} = A \exp(i\phi)$ is the actual received complex acoustic pressure field, $\mathbf{p}_0$ is the received field in the absence of scattering, A is the received pressure amplitude, and ϕ is the received phase. The acoustic pressure p (without bolding) discussed in Section 2 is the real part of $\mathbf{p}$.

5. CONCLUSION

Acoustic FDTD simulation (and the increasing capabilities of modern parallel-processing computers) makes possible highly detailed calculations of sound propagation through dynamic atmospheric fields. In this paper, we presented 3D calculations of low-frequency sound propagation through an ABL large-eddy simulation. We also used acoustic FDTD in combination with kinematically generated turbulence fields to test theoretical predictions for wavefields propagating through turbulence. Similar simulations hold promise for elucidating scattering phenomena affecting atmospheric remote sensing systems.

Acknowledgments: Funding for this project was provided by the DoD High Performance Computing Modernization Office's Common High-Performance Scalable Software Initiative and the U.S. Army Engineer Research and Development Center.

REFERENCES

Attenborough, K. et al., 1995: Benchmark cases for outdoor sound propagation models. *J. Acoust. Soc. Am.*, **97**, 173–191.

Blumrich, R. and D. Heimann, 2002: A linearized Eulerian sound propagation model for studies of complex meteorological effects. *J. Acoust. Soc. Am.*, **112**, 446–455.

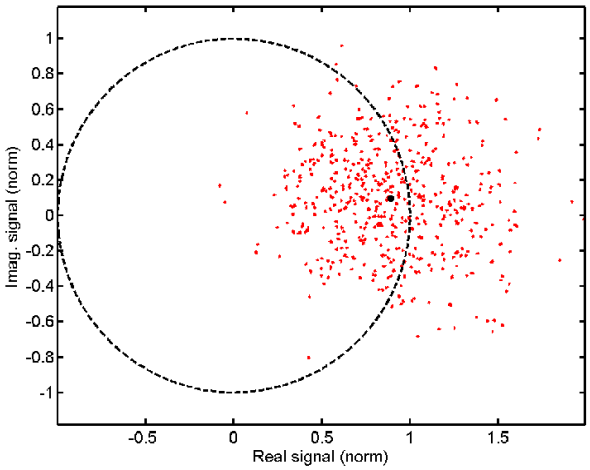

FIG. 7: Samples of the complex acoustic pressure at 500 virtual microphones for an FDTD calculation of sound propagation through kinematic turbulence. The small red dots (actually short lines) are the time-varying pressure samples. The large black dot is the complex mean. The dashed line shows the unit circle, which represents zero-amplitude fluctuation.

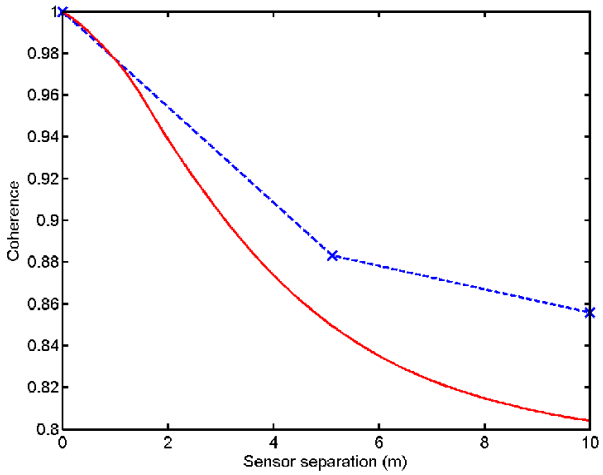

FIG. 8: Sound-field coherence calculated by averaging pairs of microphones after propagation through the kinematic turbulence. Solid curve is the theoretical prediction and X's are the FDTD results.

Botteldooren, D., 1994: Acoustical finite-difference time-domain simulation in a quasi-Cartesian grid. *J. Acoust. Soc. Am.*, **95**, 2313–2319.

Goedecke, G., V. E. Ostashev, D. K. Wilson, and H. J. Auvermann, 2004: Quasi-wavelet model of von Kármán spectrum of turbulent velocity fluctuations. *Boundary-Layer Meteorol.*, **112**, 33–56.

Ishimaru, A., 1978: *Wave Propagation and Scattering in Random Media*. Academic Press, New York.

Liu, L. and M. L. Moran, 2002: Acoustic wave propagation in atmospheric boundary layer above rough terrain. *J. Acoust. Soc. Am.*, **111**, 2378–2379. Abstract only.

Ostashev, V. E., 1997: *Acoustics in Moving Inhomogeneous Media*. E & FN Spon, London.

Ostashev, V. E., D. K. Wilson, L. Liu, D. F. Aldridge, N. P. Symons, and D. H. Marlin, 2004: Equations for finite-difference, time-domain simulation of sound propagation in moving media and numerical implementation. *J. Acoust. Soc. Am.* submitted.

Salomons, E. M., 2001: *Computational Atmospheric Acoustics*. Kluwer, Dordrecht.

Salomons, E. M., R. Blumrich, and D. Heimann, 2002: Eulerian time-domain model for sound propagation over a finite-impedance ground surface. Comparison with frequency-domain models. *Acust. Acta Acust.*, **88**, 483–492.

Sullivan, P. P., J. C. McWilliams, and C.-H. Moeng, 1994: A subgrid-scale model for large-eddy simulation of planetary boundary-layer flows. *Boundary-Layer Meteorol.*, **71**, 247–276.

Sullivan, P. P., J. C. McWilliams, and C.-H. Moeng, 1996: A grid nesting method for large-eddy simulation of planetary boundary-layer flows. *Boundary-Layer Meteorol.*, **80**, 167–202.

Symons, N., D. Aldridge, D. K. Wilson, D. Marlin, and V. Ostashev, 2003: 3D finite-difference simulation of acoustic waves in turbulent moving media. *J. Acoust. Soc. Am.*, **114**, 2440. Abstract only.

Wilson, D. K. and L. Liu, 2004: Finite-difference, time-domain simulation of sound propagation in a dynamic atmosphere. Technical Report ERDC/CRREL TR-04-12, U.S. Army Cold Regions Research and Engineering Laboratory, 72 Lyme Rd, Hanover, NH 03755-1290.

Wilson, D. K., V. E. Ostashev, G. H. Goedecke, and H. J. Auvermann, 2004: Quasi-wavelet calculations of sound scattering behind barriers. *Appl. Acoust.*, **65**, 605–627.

Yee, K. S., 1966: Numerical solution of initial boundary value problems involving Maxwell's equations in isotropic media. *IEEE Trans. Antennas and Propagation*, **14**, 302–307.